NANO LETTERS

pubs.acs.org/NanoLett

Lithium Insertion In Silicon Nanowires: An ab Initio Study

Qianfan Zhang,[†] Wenxing Zhang,[†] Wenhui Wan,[†] Yi Cui,*[,‡] and Enge Wang*[,†,§]

[†]Institute of Physics, Chinese Academy of Sciences, Beijing 100190, China, [‡]Department of Materials Science and Engineering, Stanford University, Stanford, California 94305, and [§]School of Physics, Peking University, Beijing 100871, China

ABSTRACT The ultrahigh specific lithium ion storage capacity of Si nanowires (SiNWs) has been demonstrated recently and has opened up exciting opportunities for energy storage. However, a systematic theoretical study on lithium insertion in SiNWs remains a challenge, and as a result, understanding of the fundamental interaction and microscopic dynamics during lithium insertion is still lacking. This paper focuses on the study of single Li atom insertion into SiNWs with different sizes and axis orientations by using full ab initio calculations. We show that the binding energy of interstitial Li increases as the SiNW diameter grows. The binding energies at different insertion sites, which can be classified as surface, intermediate, and core sites, are quite different. We find that surface sites are energetically the most favorable insertion positions and that intermediate sites are the most unfavorable insertion positions. Compared with the other growth directions, the [110] SiNWs with different diameters always present the highest binding energies on various insertion locations, which indicates that [110] SiNWs are more favorable by Li doping. Furthermore, we study Li diffusion inside SiNWs. The results show that the Li surface diffusion has a much higher chance to occur than the surface to core diffusion, which is consistent with the experimental observation that the Li insertion in SiNWs is layer by layer from surface to inner region. After overcoming a large barrier crossing surface-to-intermediate region, the diffusion toward center has a higher possibility to occur than the inverse process.

KEYWORDS Silicon nanowire, anode, lithium ion battery, ab initio simulation, binding energy, diffusion barrier

Silicon nanowires (SiNWs) have attracted much attention for many applications, such as field effect transistors,[1−3] nanosensors,[4−6] and solar cells.[7−9] These applications take advantage of the high crystallinity and/or large surface area of SiNWs. Excitingly, SiNWs have recently been demonstrated as ultrahigh capacity lithium ion battery negative electrodes,[10] which opens up exciting opportunities for energy storage devices. Silicon has the highest known specific charge capacity (4200 mAh/g), which is ∼10 times larger than that of the graphite carbon used in existing technology.[11] However, the 300% volume expansion upon lithium insertion has caused pulverization or mechanical fracture in micrometer particle and bulk Si. The success of using SiNWs lies in their facile strain relaxation without mechanical breaking, efficient electron transport along their long axis, and large lithium ion flux due to their large surface area. Since the important demonstration of SiNWs as lithium ion battery anodes, a variety of Si nanostructure morphologies has been demonstrated to overcome the mechanical breaking issues and perform well as anodes. Si nanostructures shown to exhibit good performance include crystalline-amorphous core−shell Si NWs,[12] carbon-amorphous Si core−shell NWs,[13] Si nanotubes,[14] porous Si particles,[15] and an ordered macroporous carbon-Si composite.[16] However, experimental investigation has mainly been focused on electrochemical cycling of Si−Li compounds and phase transitions during Li insertion; all the Si−Li phases were found when the system is rich in Li atoms.[10,17] Although the Si−Li compound can be accurately analyzed, the fundamental interaction between Li and Si atoms and the microscopic dynamic process during Li insertion still remain unknown.

On the theoretical side, there have been studies on electronic properties,[18−20] surface effects,[21,22] B or P doping,[23] and phonon modes[24,25] in different types of pure SiNWs using first-principle schemes or the tight-bonding model. A general conclusion is that as the diameter of a SiNW decreases, the quantum confinement effect is stronger. The detailed density of states analysis shows that Si atoms on different positions have different contributions to the electronic structure near the band gap, and the facet effect is significant. Therefore, we expect that such quantum confinement and surface effects will also influence the Li insertion process, especially in ultrathin SiNWs.

In the present work, we have investigated single Li atom insertion in various types of SiNWs with different diameters and along different growth directions using first principle calculations. We found that different types of SiNWs will introduce different binding energies, and as the diameter of the SiNW grows, the Li binding energy gradually increases to the bulk value. Among them, the binding energies of [110] SiNWs become bulklike the fastest. Different insertion sites in the same SiNW, which can be classified as surface,

* To whom correspondence should be addressed, yicui@stanford.edu (Y.C.); egwang@iphy.ac.cn (E.W.).
Received for review: 12/14/2009
Published on Web: 08/03/2010

DOI: 10.1021/nl904132v | *Nano Lett.* **2010,** *10,* 3243–3249

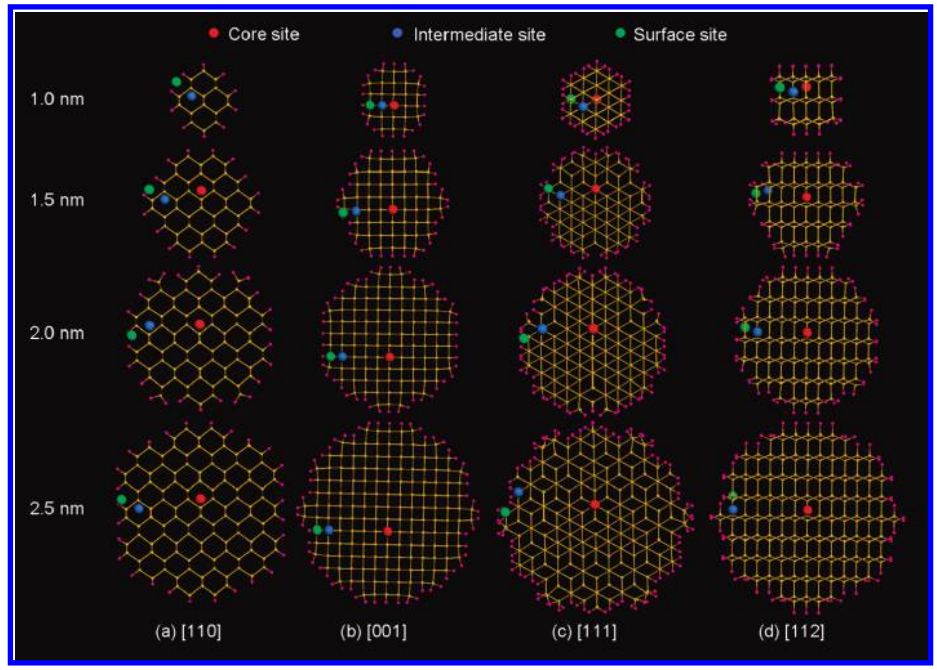

FIGURE 1. The cross planes of SiNWs with axis oriented to (a) [110], (b) [001], (c) [111], and (d) [112], and the diameters $d \approx 1.0$, 1.5, 2.0, and 2.5 nm. Si and H atoms are represented by small yellow and pink balls, respectively. The typical core, intermediate, and surface sites are shown as larger red, blue, and green balls, respectively.

intermediate, and core sites, induce different Li binding energies; in general, surface sites are the most stable insertion positions while the intermediate sites are the most unstable. Compared with the other growth directions, the [110] SiNWs with different diameters always present the highest binding energies on various insertion locations. It means that [110] SiNWs are more favorable by Li doping. Single Li diffusion in different SiNWs has been also studied. Our results show that diffusion in the surface region is relatively easy due to low barriers between surface sites, while the diffusion in the core region is relatively hard. The surface to bulk diffusion meets a large initial barrier crossing surface-to-intermediate region, after which the diffusion toward center has a high possibility to occur.

The first principles calculations were performed using the Vienna ab initio simulation program (VASP)[26,27] in the framework of density functional theory (DFT). Four types of SiNWs with the long axis along the [110], [001], [111], and [112] directions were investigated with diameters (d) ranging between 1.0 to 2.5 nm. The cross-sectional planes of these SiNWs are shown in Figure 1. Si atoms on the surface are passivated by H atoms to make sure that all the Si atoms have the coordinate number of four and no dangling bond exists. The vacuum between a SiNW and its image exceeds 18 Å, while the distance between an inserted Li atom and its image is no less than 11 Å along the long axis direction. Such a system is large enough to avoid any artificial interaction between images after our careful tests. We used the projector augmented plane waves (PAW)[28] method and the generalized gradient approximation (GGA) exchange-correlation developed by Perdew and Wang (PW91).[29] A plane wave cutoff of 400 eV and k-point mesh of $1 \times 1 \times 3$ in the Monkhorst–Pack sampling scheme were used.[30] The structural relaxation was performed using the conjugated gradient minimization method to make sure the force on each atom is less than 0.02 eV/Å. Furthermore, we have tested the results by using various methods with PBE xc functional, local density approximation (LDA), and ultrasoft pseudopotential, and the tendency is the same with that obtained by PAW GGA (PW91).

The Kohn–Sham band structures of all thin SiNWs were calculated first. The results indicate that when $d < 2.5$ nm, [110], [001], and [111] SiNWs are direct band gap semiconductors with both the valence band maximum (VBM) and the conduction band minimum (CBM) at the Γ point ($k = 0$), while the series of [112] SiNWs are indirect semiconductors, with the VBM at the Γ point as well, but the CBM is at the boundary of Brillouin zone. Here $k = (2/3)^{1/2}\pi/a$ where a is the lattice constant of crystalline Si. The band gaps of various SiNWs are shown in Figure 2. The calculated band gaps are all about 0.3–0.4 eV smaller compared with the results obtained by Zhang's simulation using the tight-binding model[24] in which the parameters are fitted by DFT simulation considering GW correction.[31] Such underestimation of band gap is a known artifact of traditional DFT.[32] The band gap increases when the diameter decreases due to significant quantum confinement effects in ultrathin SiNWs. The series of [110] SiNWs always have the narrowest band gap. The bandgap value is 0.91 eV when $d \approx 2.5$ nm, which is only 0.24 eV larger than that in bulk Si. The band gaps of [001], [111], and [112] SiNWs are 0.24, 0.16, and 0.15 eV larger than the [110] SiNW value for $d \approx 2.5$ nm, respec-

DOI: 10.1021/nl904132v | *Nano Lett.* **2010,** *10,* 3243–3249

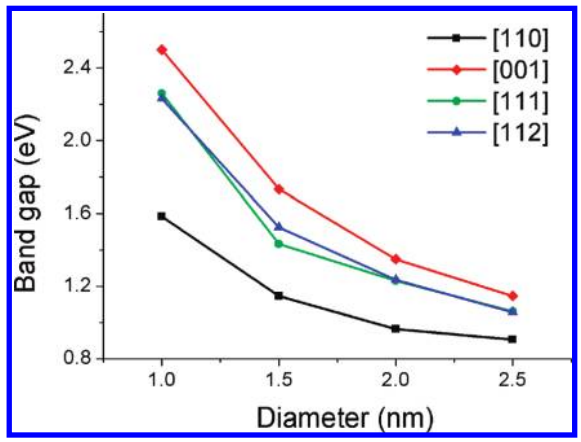

FIGURE 2. Band gaps of [110], [001], [111], and [112] SiNWs with wire diameters $d \approx 1.0$, 1.5, 2.0, and 2.5 nm.

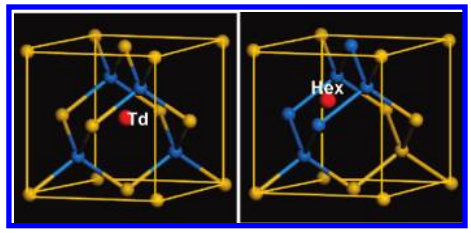

FIGURE 3. Illustration of (left) tetrahedral (Td) and (right) hexagonal (Hex) sites in bulk Si as represented by red balls. Blue balls represent the neighboring Si atoms.

tively. The series of [001] SiNWs have the widest band gap. These results suggest that the electronic properties in [110] SiNWs become bulk-like more quickly than other types of SiNWs with increase of NW diameter.

In bulk silicon, the most stable position for Li atom insertion is a tetrahedral (Td) site with four nearest Si atoms as shown in Figure 3a, and the corresponding binding energy of a single Li atom is 1.36 eV. In SiNWs, however, there are many nonequivalent stable sites because the periodicity in the cross-sectional plane of SiNWs is lost. For the convenience of discussion, these sites are classified into the following three kinds: (1) surface site (S site), the site has less than four coordinating Si neighbors; (2) intermediate Td site (I site), the site has four coordinating Si atoms and at least one is surface atom; and (3) core Td site (C site), the site is inside the SiNW and has four core Si coordination atoms. The binding energy, E_b, is defined as the energy difference between the Li-inserted SiNW system (E_{tot}) and the summation of single Li atom (μ_{Li}) and pristine SiNW (E_{SiNW})

$$E_b = E_{SiNW} + \mu_{Li} - E_{tot}$$

It is nearly impossible to exhaust complete binding energy computations because of too many nonequivalent insertion sites even in SiNWs with diameter $d \approx 1.0$ nm. To calculate E_b in each type of SiNW, we extracted one typical core site,

TABLE 1. Binding Energies (E_b) at Typical Surface (S), Intermediate (I), and Core (C) Sites in [110], [001], [111], and [112] SiNWs with Diameters $d \approx 1.0$, 1.5, 2.0, and 2.5 nm

		E_b (eV)			
SiNW	type of site	1.0 nm	1.5 nm	2.0 nm	2.5 nm
[110]	C		1.22	1.34	1.35
	I	0.88	1.07	1.23	1.26
	S	1.21	1.43	1.67	1.73
[001]	C	0.59	1.03	1.12	1.24
	I	0.47	0.94	0.91	1.17
	S	1.03	1.33	1.38	1.59
[111]	C	0.52	0.93	1.04	1.14
	I	0.40	0.78	0.82	1.03
	S	0.91	1.07	1.29	1.45
[112]	C	0.60	0.97	1.10	1.26
	I	0.47	0.83	0.91	1.18
	S	1.00	1.34	1.46	1.61

intermediate site, and surface site, respectively, as marked by red, blue, and green balls in Figure 1. The results are summarized in Table. 1. A typical C site is the stable position near the center of a SiNW, while a typical S site is defined as a site that is located on a surface with neither a too high nor too low coordination number and can be served as representative of a common case. To investigate the binding energy variety at numerous nonequivalent sites, we present the results of a Li atom in [110] and [111] SiNWs with diameter $d \approx 1.5$ nm. The systems under study have structurally diverse insertion sites. For each type of SiNW, binding energies on nine different sites have been calculated. The insertion sites are displayed in Figure 4, and E_b values are summarized in Table. 2.

As shown in Table 1, the binding energy becomes larger when the diameter of the SiNWs increases. It is found that E_b on the C site approaches the bulk value when the diameter changes from $d \approx 1.0$ to 2.5 nm. That means when the SiNW

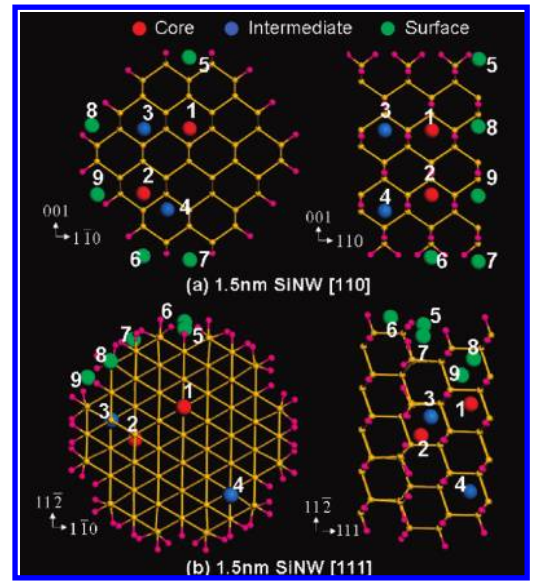

FIGURE 4. Various Td sites in [110] (a) and [111] (b) SiNWs with a diameter of 1.5 nm. The left and right figures are the cross and the side planes. Two C sites (Sites 1 and 2), two I sites (Sites 3 and 4) and five S sites (Sites 5−9) are shown. Their E_b results are given in Table 2.

DOI: 10.1021/nl904132v | *Nano Lett.* **2010,** *10,* 3243–3249

TABLE 2. Binding Energies (E_b) and Coordinate Number (Divided into Core Si Number and Surface Si Number) at Various Nonequivalent Td Sites in 1.5 nm [110] and [111] SiNWs Where the Different Sites Are Labeled As Those in Figure 4

SiNW	site	type	E_b (eV)	coordinate number
[110]	1	C	1.22	(4, 0)
	2	C	1.23	(4, 0)
	3	I	1.12	(3, 1)
	4	I	1.08	(3, 1)
	5	S	1.65	(2, 0)
	6	S	0.92	(0, 1)
	7	S	1.20	(0, 2)
	8	S	1.43	(0, 3)
	9	S	1.40	(1, 0)
[111]	1	C	0.93	(4, 0)
	2	C	0.92	(4, 0)
	3	I	0.82	(3, 1)
	4	I	0.78	(3, 1)
	5	S	1.35	(2, 1)
	6	S	1.02	(0, 2)
	7	S	1.19	(1, 2)
	8	S	1.09	(0, 3)
	9	S	1.07	(1, 0)

is very thin, the Li interstitial can be greatly influenced by the surface atoms even on the so-called C sites. The quantum confinement induces electron wave function localization in ultrathin SiNWs and results in weaker interaction between Li defect and host.[33,34] Compared with other types of SiNWs, the series of [110] SiNWs always induce the highest binding energies on various insertion locations, and the E_b value almost reaches the same as that in bulk Si as soon as the diameter approaches $d \approx 2.0$ nm. The result is consistent with electronic band structure calculations, which shows that the band gap of [110] SiNWs approaches the bulk value much more quickly than other orientations. The [111] SiNWs show the lowest binding energies, and the E_b value on the C site is only 1.14 eV when $d \approx 2.5$ nm, about 200 meV smaller than the calculated bulk value. Our results indicate that [110] SiNWs are more favorable by Li doping.

It can be clearly seen that in the same SiNW, the binding energy on typical S site is always the highest, while that on the I site is always the smallest, regardless of the size of SiNWs. The higher binding energy on a typical S site is ascribed to the shortage of Si atom neighbors. In fact, we find that the Li atom has the tendency to stay away from neighboring Si atoms in bulk Si because of large radius of the Li atom (1.6 Å). The distance between a Li atom on a Td site and the nearest Si atoms is about 2.45 Å, which is smaller than the summation of the Li and Si radii, 2.7 Å. However, on S sites, such mismatch can be overcome because of the lack of Si neighbors in some directions, and according to our statistics, the bond lengths between Li and the nearest Si atoms are between 2.60 and 2.73 Å.

The primary difference between the I site and the C site is the existence of neighboring Si surface atoms for a Li interstitial on I sites, and that distinction causes the binding energy to be about 80−220 meV lower than that on C sites. As shown in Figure 4 and Table 2, the energy difference between two C sites, marked as Site 1 and 2 in both SiNWs, is no more than 10 meV, even when Site 1 is located near the center while Site 2 is much nearer to the surface. Site 2 and Site 3 are adjacent Td sites, but their E_b values have a difference of 100 meV because they belong to different kinds of Td insertion positions. The results strongly indicate that the bonding scheme of Si neighbors plays a critical role in Li insertion. To elucidate this role, we studied the charge transfer between Li and neighboring Si. The charge density difference $\Delta\rho$ is defined as

$$\Delta\rho = \rho[\text{Li/SiNW}] - \rho[\text{Li}] - \rho[\text{SiNW}]$$

$\Delta\rho$ along Si−Li bond lines in 1.5 nm [110] SiNWs are calculated when interstitial Li atoms are inserted into typical C and I sites, as shown in Figure 1, respectively. The $\Delta\rho$ curves are shown in Figure 5a. Bond Si1−Li1 represents the C site case while Bond Si2−Li2 and Si3−Li2 represent interstitial Li bonds with core Si and surface Si neighbors on I sites, respectively. The $\Delta\rho$ curves of Bond Si1−Li1 and Bond Si2−Li2 almost coincide but the charge transfer amount

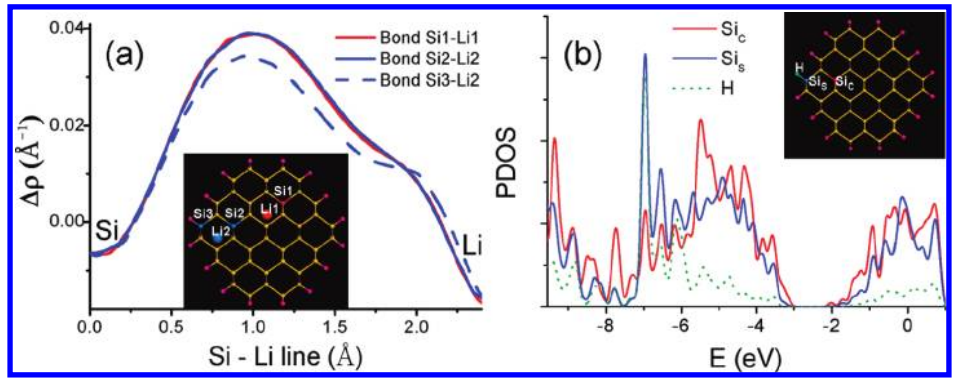

FIGURE 5. (a) Charge density difference $\Delta\rho$ along Si−Li bonds. The inset is the [110] SiNW cross plane, which illustrates the bond Si1−Li1 when Li is on the core (red) site, and bond Si2−Li2 and bond Si3−Li2 when Li is on the intermediate (blue) site. (b) Partial density of state for surface Si atom (Si_S) and core Si atom (Si_C) are shown by blue and red curves, respectively, and the PDOS of H binded to Si_S is also plotted for reference. The inset is the [110] SiNW cross plane, which illustrates the positions of Si_S, Si_C, and H.

DOI: 10.1021/nl904132v | *Nano Lett.* **2010,** *10,* 3243–3249

TABLE 3. Energy Difference between I Site and C Site ($\Delta E_{IC} = E_I - E_C$) When the Neighboring Surface Si Atom for I Site Binded with Different Types of Passivation Atoms[a]

X	ΔEN	ΔE_{IC} (eV)
H	0.3	0.15
F	2.1	0.24
Cl	1.7	0.22
Br	1.5	0.21
Na	−1.0	−0.20
K	−0.9	−0.22

[a] ΔEN represents electronegativity difference between passivation atoms and Si atom ($\Delta EN = EN_X - EN_{Si}$).

along Bond Si3−Li2 is smaller in the middle and the peak is 12% lower. The comparison demonstrates that the electron distribution between neighboring core Si and Li remains almost the same whether it is on the C or I site, but less electron drift occurs from Li to surface Si. Therefore, the interaction between surface Si and Li atoms is weaker than that between core Si and Li atoms. To clarify this point, we analyzed the partial density of state (PDOS) of surface Si atom (Si_S) and core Si atom (Si_C) and show the results in Figure 5b. It can be clearly seen that the PDOS of Si_S has sharp peaks in the range of −6.8∼ −6.2 eV, which is caused by strong interaction between Si_S and binded H atom. However, the PDOS of Si_C is generally larger in other range comparing with that of Si_S. The distinction indicates that Si_S deviates from sp^3 hybridization and the wave function trend to distribute toward Si_S-H bond, which weakens the wave function overlapping and then the interaction between Si_S atom and I-sited Li defect.

In most theoretical simulations on SiNWs, H atoms were served as passivation element. However, the interface is very complicated in experiments, where SiNWs may bind with oxide, metal, or hydrogen.[35,36] To simulate the interface, we substituted the H atom that binds with Si_S atom by a serial of halogen atoms or alkali atoms and calculated the energy difference between I site and C site. The results are shown as Table. 3. It can be clearly seen that when the electronegativity (EN) of substituted passivation element is larger and larger, I site is less and less stable comparing with C site. When EN value of surface atom is smaller than that of Si atom (Na or K atom), I site is more stable. This distinction can be attributed to the ionic nature of Si−Li bond. As the EN of surface atom increases, the electron density around Si_S decreases and the interaction between Si and Li weakens. Therefore, it suggests that the energy difference between I site and C site is not determined by confinement effect, but by the feature of interface atoms, and H-passivated SiNWs can also represent the common case when element with high EN value exists on interface, like oxygen or some transition metal.

In contrast to the C or I sites, the distinction among different S sites can be more significant. Site 5 in [110] SiNWs results in a Li binding energy 430 meV higher than that on the C site, but Site 7 in [110] SiNW leads to a Li binding energy 160 meV lower than that on the I site. The facet effect has been widely discussed in recent years and the general conclusion has been made that different facets have different contributions to the electronic properties.[21,23] However, in Li insertion investigations, we find that the binding energy of interstitial Li is almost independent of facets, and the E_b values can be quite different even in closed S sites on the same facet. That variety of binding energies is caused by distinct local environments around different S sites, including the number of nearest or second nearest Si atoms, the neighboring Si atom and H atom configuration, and its positional relationship with the Li atom. Nevertheless, we found that the E_b value is mainly determined by the Si atom coordinate number, especially the number of core Si neighbors. The Si coordinate numbers for interstitial Li divided into the number of surface and core Si neighbors are shown in the fifth column in Table 2. Under the condition of less than four Si coordinating neighbors, which can fully relax the strain resulting from short Li−Si distances, the S site binding energy becomes larger as the coordination number increases. Comparing the binding energy of different S sites (Table 2) suggests again that core Si neighbors contribute much more to binding energy.

Finally, we have investigated the barriers when an interstitial Li atom diffuses between different sites. As examples, using the nudged elastic band scheme,[37] we give the diffusion barrier along the pathways from surface to inner core for both [110] and [111] SiNWs with $d \approx 1.5$ nm in Figure 6. The corresponding energy curves are also plotted in Figure 6b,d. For both SiNWs, 1→2→3, 4→5, and 6→7 belong to intraregional surface-to-surface (S-to-S), intermediate-to-intermediate (I-to-I), and core-to-core (C-to-C) diffusion, respectively. The 3→4 and 5→6 processes represent cross-regional surface-to-intermediate (S-to-I) and intermediate-to-core (I-to-C) diffusion, while their inverse processes are I-to-S and C-to-I diffusion. The energy variations in both types of SiNWs show a similar behavior. The barrier to Li diffusion in the core region is almost the same as that in the bulk (0.58 eV), even when the SiNWs are ultrathin and the binding energy is much lower than the bulk value. That means for different types of SiNWs the quantum confinement effect has little influence on diffusion barriers as the diffusion shows a weak dependence on size. It can be clearly seen that all the S-to-S barriers are much lower, only 0.12−0.20 eV. The S-to-I barrier is very high (about 0.9 eV) crossing surface-to-intermediate region, and the I-to-C barrier is about 0.1 eV lower than the core region diffusion barrier. The I-to-I, I-to-S and C-to-I barriers are quite similar to their bulk results with a difference of no more than 40 meV. The conclusion based on large barrier distinctions in different diffusion regions indicates that the surface diffusion has a much higher chance to occur than surface to core diffusion. The result is consistent with the experimental observation that the Li insertion in SiNWs is layer by layer from surface to inner region as the Li concentration increases during the Li insertion process.[10] The energy from Site 4 to Site 7

DOI: 10.1021/nl904132v | Nano Lett. 2010, 10, 3243–3249

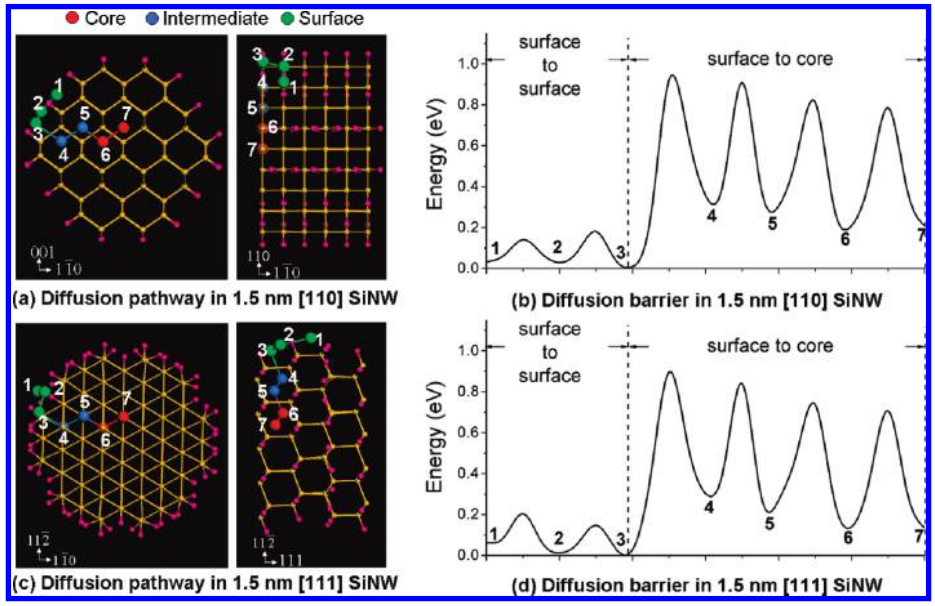

FIGURE 6. Li diffusion in 1.5 nm [110] and [111] SiNWs. (a,c) The cross (left) and side (right) view of the pathways under study. The diffusion barriers along the pathways are shown in panels b and d, respectively.

becomes lower and lower, which indicates all the barriers for Li diffusion from intermediate to inner region are smaller than those of the inverse processes. Therefore, the diffusion toward center has a high possibility to occur as soon as Li defect enters the intermediate region.

In bulk Si, the transition state between different Td stable sites is the so-called hexagonal (Hex) point, as shown in Figure 3 (b), where the Li defect has six Si neighbors. The distance between a Li defect and a neighboring Si atom is 2.37 Å, which is 0.08 Å shorter than that in the Td site. In SiNWs, the Hex point can also be classified as a surface, intermediate or core site. Only the Hex saddle point between surface stable sites has a coordinate number lower than six, and according to our statistics, the Li−Si distances are in the range of 2.62−2.71 Å, which is much larger than that in intermediate or core sites. Due to the loss of Si neighbors, the motion of a Li defect can be fully relaxed during the whole S-to-S process and the barrier is much lower than that in the core region. In I-to-I or C-to-C diffusion, the saddle point has the same intermediate or core feature, while the saddle points of S-to-I and I-to-C diffusion are intermediate and core Hex sites, respectively. Therefore, the C-to-C, I-to-I, S-to-I, and C-to-I barriers are all similar to that in the bulk case. The discussion above indicates that the barrier heights are determined by both the type of Td and Hex sites and the features of their Si neighbors.

In conclusion, we have presented a systematic study of the electronic structures of various nonequivalent stable sites and the diffusion barriers of different pathways for a single Li insertion in SiNWs with different diameters along different axis orientations within the DFT framework. Various methods with PAW GGA (PW91), PBE xc functional, local density approximation (LDA), and ultrasoft pseudopotential have been used in the study. In general, the Li binding energy increases as the diameter grows and the S and I sites have the highest and lowest binding energies, respectively. Different C or I sites lead to similar E_b values, but those on S sites vary over a relatively large range. Compared with the other growth directions, the [110] SiNWs with different diameters always present the highest Li binding energies on various insertion locations. It means that [110] SiNWs are more favorable by Li doping. The diffusion barrier height has little relationship with the orientation of the SiNWs. The surface-to-surface diffusion barriers are much lower than the core to core diffusion barriers. However, the surface-to-bulk diffusion meets a large barrier crossing the surface-to-intermediate region. This result is consistent with the experimental observation that the Li insertion in SiNWs is layer by layer from the surface to the inner region as the Li concentration increases. Our ab initio study provides valuable understanding of fundamental interactions between Li and SiNWs and the microscopic process of Li insertion dynamics, especially in the clarification of quantum confinement and surface effects during Li insertion.

Acknowledgment. This work was supported by CAS and NSFC. E.W. acknowledges Stanford GCEP visiting scholar program. We also gratefully acknowledge the computational time by the Swedish agency SNAC. Y.C. acknowledges support from the King Abdullah University of Science and Technology (KAUST) Investigator Award (No. KUS-l1-001-12), Stanford GCEP, and US ONR.

REFERENCES AND NOTES

(1) Cui, Y.; Lieber, C. M. *Science* **2001**, *291*, 851.
(2) Duan, X.; Niu, C.; Sahi, V.; Chen, J.; Parce, J. W.; Empedocles, S.; Goldman, J. L. *Nature* **2003**, *425*, 274.
(3) Cui, Y.; Zhong, Z. H.; Wang, D. L.; Wang, W. U.; Lieber, C. M. *Nano Lett.* **2003**, *3*, 149.

DOI: 10.1021/nl904132v | *Nano Lett.* **2010,** *10,* 3243--3249

(4) Stern, E.; Klemic, J. F.; Routenberg, D. A.; Wyrembak, P. N.; Turner-Evans, D.; Hamilton, A.; LaVan, D. A.; Fahmy, T. M.; Reed, M. A. *Nature* **2007**, *445*, 519.
(5) McAlpine, M. C.; Ahmad, H.; Wang, D. W.; Heath, J. R. *Nat. Mater.* **2007**, *6*, 379.
(6) Park, I. Y.; Li, Z. Y.; Li, X. M.; Pisano, A. P.; Williams, R. S. *Biosens. Bioelectron.* **2007**, *22*, 2065.
(7) Tian, B. Z.; Zheng, X. L.; Kempa, T. J.; Fang, Y.; Yu, N. F.; Yu, G. H.; Huang, J. L.; Lieber, C. M. *Nature* **2007**, *449*, 885.
(8) Garnett, E. C.; Yang, P. D. *J. Am. Chem. Soc.* **2008**, *130*, 9224.
(9) Kayes, B. M.; Atwater, H. A.; Lewis, N. S. *J. Appl. Phys.* **2005**, *97*, 114302.
(10) Chan, C.; Peng, H.; Liu, G.; McIlwrath, K.; Zhang, X. F.; Huggins, R. A.; Cui, Y. *Nat. Nanotechnol.* **2008**, *3*, 31.
(11) Boukamp, B.; Lesh, G.; Huggins, R. *J. Electronchem. Soc.* **1981**, *128*, 725.
(12) Cui, L. F.; Ruffo, R.; Chan, C. K.; Peng, H.; Cui, Y. *Nano Lett.* **2009**, *9*, 491.
(13) Cui, L. F.; Yang, Y.; Hsu, C. M.; Cui, Y. *Nano Lett.* **2009**, *9*, 3370.
(14) Park, M. H.; Kim, M. G.; Joo, J.; Kim, K.; Kim, J.; Ahn, S.; Cui, Y.; Cho, J. *Nano Lett.* **2009**, *9*, 3844.
(15) Kim, H.; Han, B.; Choo, J.; Cho, J. *J. Angew. Chem.* **2008**, *47*, 10151.
(16) Esmanski, A.; Ozin, G. A. *Adv. Funct. Mater.* **2009**, *19*, 1999.
(17) Key, B.; Bhattacharyya, R.; Morcrette, M.; Seznec, V.; Tarascon, J.; Grey, C. *J. Am. Chem. Soc.* **2009**, *131*, 9239.
(18) Read, A. J.; Needs, R. J.; Nash, K. J.; Canham, L. T.; Calcott, P. D.; Qteish, A. *Phys. Rev. Lett.* **1992**, *69*, 1232.
(19) Niquet, Y. M.; Lherbier, A.; Quang, N. H.; Fernndez- Serra, M. V.; Blase, X.; Delerue, C. *Phys. Rev. B* **2006**, *73*, 165319.
(20) Sacconi, F.; Persson, M.; Povolotskyi, M.; Latessa, L.; Pecchia, A.; Gagliardi, A.; Balint, A.; Fraunheim, T.; Di Carlo, A. *J. Comput. Electron* **2007**, *6*, 329.
(21) Leao, C.; Fazzio, A.; da Silva, A. J. R. *Nano Lett.* **2007**, *7*, 1172.
(22) Xu, X.; Servati, P. *Nano Lett.* **2009**, *9*, 1999.
(23) Leao, C.; Fazzio, A.; da Silva, A. J. R. *Nano Lett.* **2008**, *8*, 1866.
(24) Zhang, W. X.; Delerue, C.; Allan, G.; Niquet, Y. M.; Wang, E. G. *Phys. Rev. B*; submitted.
(25) Thonhauser, T.; Maham, G. D. *Phys. Rev. B* **2004**, *69*, No. 075213.
(26) Kresse, G.; Hafner, J. *Phys. Rev. B* **1993**, *48*, 13115.
(27) Kresse, G.; Furthmuller, J. *Phys. Rev. B* **1996**, *54*, 11169.
(28) Blochl, P. *Phys. Rev. B* **1994**, *50*, 17953.
(29) Wang, Y.; Perdew, J. *Phys. Rev. B* **1991**, *44*, 13298.
(30) Monkhorst, H. J.; Pack, J. D. *Phys. Rev. B* **1976**, *13*, 5188.
(31) Aulbur, W. G.; Jonsson, L.; Wilkins, J. W. In *Solid State Physics*; Ehrenreich, H., Spaepen, F., Eds.; Academic: New York, 2000.
(32) Martin, R. In *Electronic Structure: Basic Theory and Practical Methods*; Cambridge University Press: Cambridge, England, 2004.
(33) Melnikov, D. V.; Chelikowsky, J. R. *Phys. Rev. Lett.* **2004**, *92*, No. 046802.
(34) Chan, T. L.; Tiago, M. L.; Kaxiras, E.; Chelikowsky, J. R. *Nano Lett.* **2008**, *8*, 596.
(35) Morales, A. M.; Lieber, C. M. *Science* **1998**, *279*, 208.
(36) Wu, Y.; Cui, Y.; Huynh, L.; Barrelet, C. J.; David, C. B.; Lieber, C. M. *Nano Lett.* **2004**, *4*, 433.
(37) Jonsson, H.; Mill, G.; Jacobsen, K. W. In *Classical and Quantum Dynamics in Condensed Phase Simulations*; Berne, B. J., Ciccotti, G., Coker, D. F., Eds.; World Scientific: Singapore, 1998.

DOI: 10.1021/nl904132v | *Nano Lett.* **2010,** *10,* 3243--3249